JOURNAL OF MATERIALS SCIENCE 29 (1994) 2704–2712

Surface roughness and impact strength of injection-moulded polystyrene

T. H. LEE*, N. J. MILLS
School of Metallurgy and Materials, University of Birmingham, Birmingham B15 2TT, UK

The formation of regular surface waves in injection moulded polystyrene was investigated as a function of the moulding conditions and the molecular weight distribution of the polymer. The injection velocity and the position of measurement relative to the gate of the mould have the greatest effect on the average roughness measured with a Talysurf machine. The packing pressure has only a minor effect in reducing the roughness. It is proposed that the waves occur if there is time for surface buckling in the fountain flow at the melt front. The waves are shown to have negligible effect on the unnotched impact strength, which is dominated by molecular orientation, so the waves merely detract from the surface appearance of the moulding.

1. Introduction

The mechanical properties of injection-moulded products are influenced by moulding conditions. The microstructural effects of the moulding process including 'frozen-in' molecular orientation [1–4] and residual stresses [5]. A poor surface finish can be produced when there is a low mould-filling rate. This is detrimental to the surface appearance of the moulding, and may also be detrimental to the mechanical properties of the moulding. The irregular surface may act as a stress concentrator and hence reduce the mechanical strength of the moulding. Polystyrene is a relatively brittle polymer and the effects of surface roughness should be more marked than, for instance, in polycarbonates.

It is difficult to vary the surface roughness of a moulding without changing its microstructure. In the present study, the effects of moulding conditions on the surface roughness are measured. The impact strength of these samples is then measured. The injection mouldings possess anisotropic mechanical properties, and this must be taken into account when considering the effects of the surface roughness. The direction of surface ridges is related to the flow direction during mould filling, so it is impossible independently to vary the direction of the ridges and of the orientation.

The surface roughness is a feature on the skin of the moulding. This is a thin layer next to the mould surface which is cooled below the glass transition temperature during the mould-filling flow. In the packing stage of the moulding cycle, the melt pressure in the full cavity is kept high. The moulding continues to cool, and the flow stresses in the stationary melt relax. The core of the moulding solidifies while the melt is stationary. There is a distribution of molecular orientation through the moulding, with high values in the skin and lower values in the core. The mould cavity pressure tends to decrease during the packing stage, and this will lead to a residual stress distribution in the moulding [6]. The compressive residual stresses in the skin are balanced by tensile residual stresses in the core. It is very difficult to change one parameter (surface roughness in this case) without changing several other parameters at the same time. Hence the impact test results must be examined critically to see whether the surface roughness is a cause of change, even if it correlates with some strength parameter.

Hogberg [7] compared the impact strength and density of the surface layer to the interior portion of polystyrene mouldings, and showed that they were inhomogeneous. Jackson & Ballman [2] found substantial anisotropy, with differences in the mechanical properties parallel and perpendicular to the injection-moulding flow direction.

2. Theory

2.1. Roughness development during mould filling

Mould filling involves the non-isothermal, non-steady flow of a compressible viscoelastic material through a flow channel of complex shape. Flow visualization studies [8] showed that there are two regimes of mould filling. One involves steady filling by a front which fills the mould cross-section, and the second involves the unstable jetting of melt from the gate through the mould. We are concerned with the steady filling mode. It is generally accepted that there is fountain flow [9–11] at the leading edge of the melt. Our microscopic observations of this region of a short-shot moulding (when the flow stops before the cavity is completely filled) shows that the surface waves have developed in this region (Fig. 1).

The cause of the waves could be a flow instability; however, this is rejected because the wave amplitude is

* *Present address*: 3531 River Road South, Kuala Lumpur 52000, Malaysia.

0022–2461

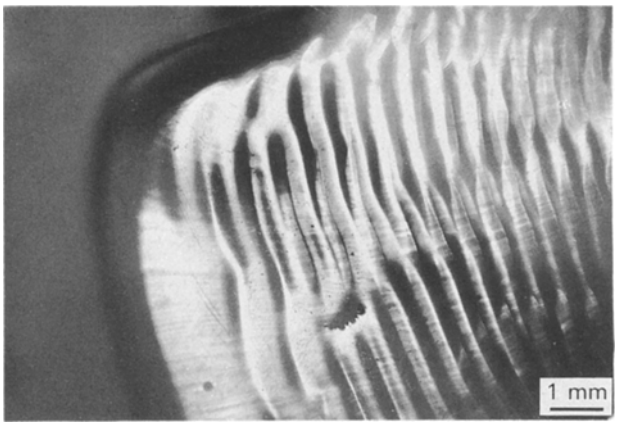

Figure 1 Bar surface of the end of a short-shot moulding showing the waves that form when injection velocity is low.

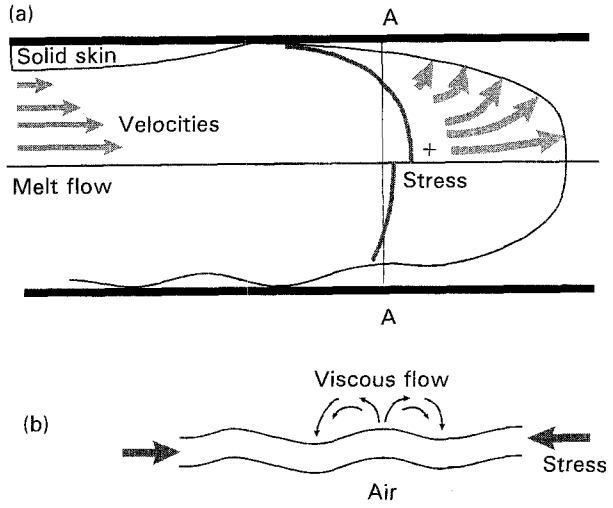

Figure 2 Flow during mould filling. (a) Upper half shows the flow pattern with fountain flow at the flow front, and melt tensile stresses across line AA; lower half shows the buckled skin and modified stress distribution. (b) Melt flow, necessary when the skin buckles.

reduced when the mould is filled fast, whereas all other flow instabilities in polymer flows become worse at high flow rates. Alternatively, the waves are a response to compressive stresses acting on the outer surface of the melt. On section AA shown in Fig. 2, there cannot be a net tensile force acting in the horizontal direction because the flow is not accelerating. If there are tensile stresses acting in the core region of the flow, these must be balanced by compressive stresses in the surface regions. During mould filling the shear flow due to the pressure gradient along the mould generates both shear and tensile stresses in the polymer melt. At the flow front the pressure is zero, and these stresses decay rapidly to zero. There is a certain time, T_f, for which the melt is in the fountain-flow region, and this will be shorter the faster the injection speed. An element of melt goes successively through a shear flow, the fountain flow, then comes to a halt in the pressurized skin of the moulding. When the flow ceases, the melt stresses relax and the melt relaxation times depend on the molecular weight distribution of the polymer.

In a radial flow from a gate into a parallel-sided cavity, there is an element of elongational flow; this causes tensile hoop stresses in the melt balanced by radial compressive stresses. The fountain flow at the flow front also has diverging streamlines, but the flow pattern is more complex than the radially symmetric case. Tensile stresses in a melt cause the polymer chains to orient in the direction of the stress, but compressive stresses in a melt could cause buckling if there is a free surface parallel to the stress. The wavelength of the buckling observed is of the order of 500 μm. An order of magnitude calculation uses the formula for the critical Euler buckling force of a strut of length L with built-in ends

$$F_c = \left(\frac{2\pi}{L}\right)^2 EI \quad (1)$$

where the melt elastic modulus $E = 1$ MPa, and $L = 0.5$ mm. The second moment of area I of a layer of width w and thickness t is $wt^3/12$ which means that the compressive stress to cause buckling is given by

$$\sigma_c = \frac{E}{3}\left(\frac{t\pi}{L}\right)^2 \quad (2)$$

If the thickness $t = 0.1$ mm in Equation 2, the melt compressive stress for buckling is 0.5 MPa. The magnitude of the buckling excursion is affected by the viscosity of melt that has to flow out of the way to allow the buckle to increase in amplitude. Hence the time for fountain flow should affect the amplitude of the waves.

The wavelength of the observed surface irregularities increases with the distance from the gate of the moulding. If Equation 2 is valid, this could be explained by saying that the surface compressive stresses are higher near the gate, and that the buckle length is the minimum allowable. If the buckle length L is low, then the distance that the melt must flow is also low (Fig. 2b). There must be some minimum energy consideration that predicts the wavelength as a function of the melt compressive stress, the viscosity of the melt and the time for which the melt element is in the fountain-flow region.

2.2. Effect of packing pressure in reducing surface roughness

During the packing stage there is a nearly uniform pressure distribution within the mould cavity. This was established by having melt pressure transducers near the gate and near the end of the mould (Fig. 3). During the packing stage (Fig. 4) the solid skin with the wave pattern on its surface is pressed against the flat steel mould wall by the melt pressure acting in the still-liquid core. The thickness of the skin will increase with time as the heat diffuses from the melt to the mould. For polystyrene in the melt, the thermal diffusivity is nearly constant with temperature and its value is 0.08 $mm^2 s^{-1}$ [12]. It is possible to calculate the temperature profiles either analytically (assuming a constant thermal diffusivity in a parallel-sided slab) or by finite-difference methods (when the temperature

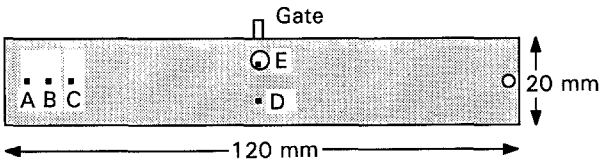

Figure 3 Plan view of the moulded bar. Letters show the positions where roughness was measured, and zeros the locations of the cavity pressure transducers.

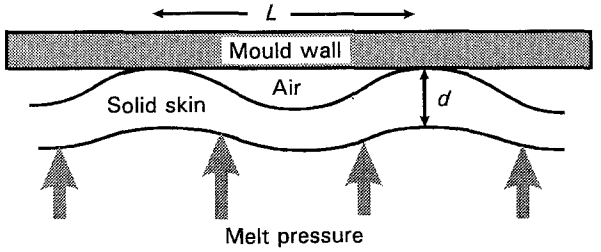

Figure 4 During the packing phase, the melt pressure acts to bend the buckled solid skin of the moulding.

dependence of the diffusivity can be incorporated into the calculations). For the present analysis it is sufficient to say that the thickness of the solid layer increases with the square root of the total contact time, c, between the melt and the mould. Using a melt temperature of 200 °C, a mould temperature of 30 °C and the condition that the polystyrene becomes glassy when its temperature is reduced to the heat-distortion temperature of 80 °C, it was calculated, using the methods described in [13], that

$$s = 0.35c^{1/2} \tag{3}$$

where the time is in seconds and the skin thickness is in mm.

Although the skin thickness has been increasing since the melt contacted the mould, the packing pressure does not come into play until the mould is full. This means that the skin thickness can be considerable near the gate. Fig. 1 shows the analysis of the bending of the skin as that of a beam of depth d and width b under a uniform load from the pressure p. The initial shape of this beam is sinusoidal with an amplitude A. The elastic deflection of this beam cannot exceed the initial separation from the mould wall, and it is of interest to see whether the pressure can flatten the skin against the mould wall. The bending moment distribution of a beam, uniformly loaded by a force of magnitude pb per metre length and supported at intervals L, is parabolic and the central deflection, x, is given by

$$x = \frac{pbL^4}{128EI} = \frac{3pL^4}{32Ed^3} \tag{4}$$

where d is the depth of the beam. Substituting typical values of $L = 0.5$ mm, $d = 0.3$ mm and $E = 3$ GPa, and a melt pressure of 20 MPa, gives a central deflection of 1.3 μm. Hence a skin thickness which only reflects a 1 s contact with the mould wall will deflect less than the typical wave amplitude of 8 μm. This means that the melt pressure may be insufficient to elastically 'iron out' the surface roughness, and the packing flow will not put extra polymer locally behind the deformed skin. As the cooling process proceeds, the solid-layer thickness increases and the 'beam' elastic deflection will decrease. If the scale of the waves is reduced, with the amplitude being proportional to the wavelength, the thickness of the skin becomes of the same magnitude as the wavelength. This will then mean that simple beam-bending theory cannot be used to calculate the elastic deflections.

2.3. Stress concentration effect of surface roughness

The surface roughness profile of the specimen looks like a series of parallel regularly spaced notches. At the tip of a single notch of radius of curvature r and length a in an elastic material, the maximum stress σ_m is given by

$$\sigma_m = \sigma_0[1 + (a/r^{1/2})] \tag{5}$$

where σ_0 is the applied stress. This formula is derived for a single central ellipse-shaped hole in a sheet; a is the semi axis of the ellipse and r is the radius of curvature of the end of the ellipse. It is doubtful if it is accurate for shallow surface waves, but it will give an order of magnitude for the stress concentration factor q, which is defined by σ_m/σ_0. The spacing b of the surface notches is approximately 50 times the depth of the notches, which means that the notches do not reduce the stress concentration at the neighbouring notch. Substituting typical values of $A = 9$ μm and $b = 400$ μm from the surface profile of the injection moulded bars into the equation for a sinusoidal surface wave gives the minimum radius of the notch as $r = 450$ μm and $q = 1.14$. This value is insignificant, as scratches in the mould surface will produce higher q values.

2.4. Analysis of Izod impact tests on unnotched bars

In an instrumented Izod impact test, the force exerted by a swinging pendulum as it strikes a specimen is measured as a function of time. For polystyrene, crazing occurs before failure in unnotched bars. Mills & Zhang [14] showed that stress–strain curves at high strain rates could be calculated from Izod impact tests on unnotched bars. The analysis used was based on the assumption that the stress distribution across the cross section is linear, with a zero stress at the mid plane (Fig. 5). The moment of this stress distribution is related to the external moment from the force F, from the nose of the pendulum acting at distance L above the clamping point. The moment is FL at the level of the top of the specimen clamp. The maximum stress in the bar (on the surface at the level of the clamp) is calculated on the assumption that the bar is elastic, using

$$\sigma = \frac{12FL}{bd^3}y \tag{6}$$

where y is the distance from the neutral surface, b is the breadth and d the depth of the bar.

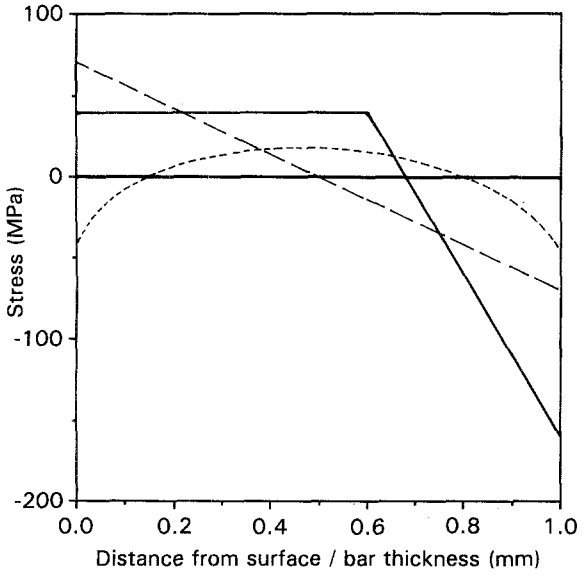

Figure 5 Stress variation through the thickness of the bent polystyrene bar. (———) Variation due to crazing at a 40 MPa stress on the tensile side for a craze length 60% of the thickness; (– – – –) assumed elastic stress variation for the same bending moment; (- - - - - - - -) residual stress distribution due to injection moulding.

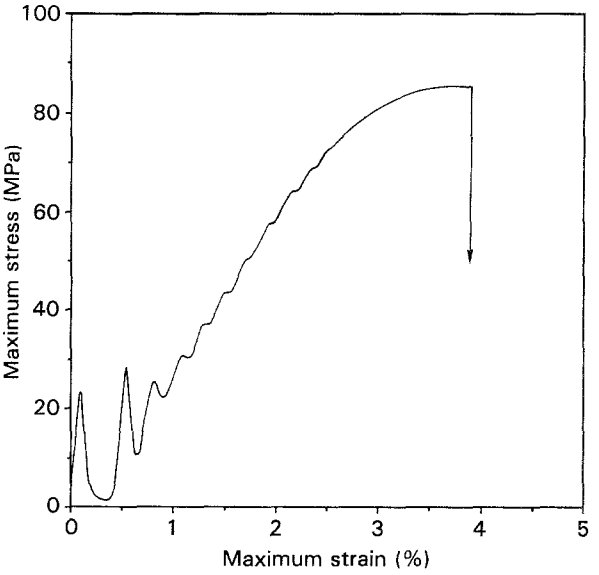

Figure 6 Maximum stress against maximum strain graph computed for unnotched Izod impact tests for the NMWD polystyrene, injection velocity 1, packing pressure 3%.

If the polymer crazes, this linear stress distribution is no longer valid. The craze stress in slowly loaded polystyrene is ~ 40 MPa, and studies of the stress distribution on the surface of a craze conclude that the stress is uniform except at the craze tip [15]. The stress distribution in the partly crazed bar is shown in Fig. 5. The compressive yield stress of polystyrene is approximately 120 MPa at moderate strain rates, and will be considerably higher at impact strain rates. Hence the assumption is made that the compressive side of the bar is still elastic. When the stress–strain data are calculated from the Izod test (see Fig. 6) it is assumed that Equation 6 is valid.

A further complication is the residual stress distribution shown in Fig. 5. This arises from the injection moulding process and is shown here as the parabolic approximation. When the residual stresses are added to the elastic bending stresses, it may mean that the maximum stress occurs below the surface of the bar. However when crazing occurs this will limit the tensile stress, and it is unlikely that the residual stresses will significantly alter the bending moment for fracturing the bar.

3. Materials and processing

3.1. Materials

Two grades of polystyrene were used in this study: a 'narrow' molecular weight distribution (MWD) polystyrene produced by BP (UK) as grade HF555 20020 NMW (the code 555 means rigid, high impact strength and high heat-distortion temperature); and a conventional MWD PS produced by Montedison, Italy, as Edistar grade FA 20010. The results of a gel permeation chromatograph MWD determination carried out by RAPRA Technology Ltd are shown in Table I.

The differences between the two polymers lies in the low molecular weight region of the MWD. Experimental measurements of melt elasticity have shown [16] that this increases as the 3.5th power of M_z/M_w. On this basis it is expected that the two polymers will have the same level of melt elasticity. The M_w values are nearly identical, so it is expected that the low-shear-rate melt viscosities will also be identical. There is more material with molecular weights in the range 1000 to 10000 in the Edistar polymer, so the surface lubrication of the melt as it flows into the mould may be better.

TABLE I GPC molecular weight analysis

Sample	Run no.	M_w	M_z/M_w	M_w/M_n
Edistar	1	248000	2.21	5.5
	2	243000	2.27	5.7
BP	1	243000	2.16	3.4
	2	242000	2.11	3.3

3.2. Processing

The injection moulding was carried out on a Battenfeld KSD machine of 23 tonnes clamping force. The mouldings were in the form of rectangular plaques of dimensions 120 × 20 × 4 mm, with the gate midway along the 120-mm side. The nozzle, barrel and hopper zone temperatures were 200, 200 and 180 °C, respectively, while the mould temperature was 30 °C. A series of different moulding conditions was used in this study. The main injection moulding variables were injection velocity and packing pressure. The machine will inject at the specified velocity unless the set injection pressure is so low that this limit is reached, and this limits the velocity. The details are given in Table II.

The injection velocities are in the arbitrary units used to control the machine. A velocity of 1 unit means that it takes 1.29 s to fill the cavity, whereas a velocity of 7 units (the maximum) means the fill time is 0.18 s. Similarly the pressure settings are percentages

TABLE II Summary of processing conditions

Sample code	V_{inj}	P_{inj} (%)	P_{pack} (%)	Max pressure (bar)	Thickness shrinkage (%)
NA	1	12	3	86	4.8
NB	1	12	5	93	
NC	1	12	20	130	4.4
ND	1	12	30	190	4.4
NE	1	12	40	330	3.7
NF	1	12	60	515	2.5
NH	7	40	10	110	4.7
WA	1	15	10	93	5.4
WB	1	15	15	106	5.3
WC	1	15	20	136	5.3
WD	1	15	30	199	5.1
WE	1	15	40	334	5.0
WF	1	15	50	405	4.8
WG	1	15	60	538	4.0
WJ	6	40	20		

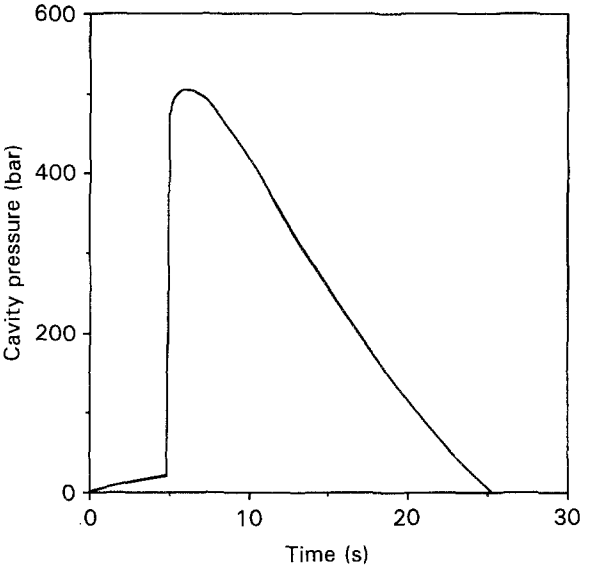

Figure 7 Mould pressure near the gate against time during the injection and packing stage for sample NF, with injection velocity 1 and packing pressure 60%.

of the theoretical melt pressures in the injection cylinder, with 100% being equivalent to 1400 bar. The pressure losses in the nozzle, sprue and feeder system means that the peak cavity pressures are lower than the cylinder pressures. In the cases where the cavity pressures were monitored as a function of time, the peak values are included in Table II. A calibration graph showed that each 1% of packing pressure corresponded to approximately 9 bar pressure at the transducer near the gate. The main effect of increasing the packing pressure is to feed more material into the mould and decrease the shrinkage of the moulding in the thickness direction.

Fig. 6 shows a cavity pressure trace for sample NF. There is a 20-bar pressure build-up at the pressure transducer near the gate before the mould is filled, then a sudden pressure jump to the packing pressure. The machine function switches from inject to pack when the cavity pressure reaches 40 bar. The shear stress at the wall of the mould can be calculated from the pressure gradient along the mould multiplied by the half thickness of the mould. It is 66 $kN\,m^{-2}$ when the mould is nearly full at $V = 1$. The slow decay in the cavity pressure in Fig. 6 for 20 s after the peak is due to solidification and shrinkage. The sprue and gate will freeze at a time of approximately 7 s; this was established by increasing the packing time until no sudden fall occurred in the cavity pressure when the packing pressure was switched off.

4. Results

4.1. Surface roughness

The mouldings were measured at the positions shown in Fig. 3, at 6, 12 and 18 mm from the left end of the specimens (positions A, B and C, respectively). Measuring positions D and E were located at 14 and 8 mm from the gate, respectively, in the middle of the bar. The surface waves are shown in Fig. 1, on the surface of a short-shot moulding. The amplitude and wave form of the roughness was measured with a Rank Taylor Hobson 'Talysurf 5'. The direction of travel of the probe is normal to the waves on the surface. Profile graphs are shown in Fig. 8 with the vertical amplitude of the wave exaggerated by a factor of 250. The profile graphs are produced by a stylus at a high voltage writing onto conducting heat-sensitive paper. It can be seen that the waveform is close to sinusoidal but the wavelength and the amplitude vary with the measurement position.

The Talysurf samples the surface shape over a length of 5 mm and calculates the average roughness parameter. R_a is defined by calculating the area between the trace and the mean height (ignoring the sign of the deviation) then dividing this by the sampling length. For a sine wave, R_a would be equal to $2/\pi$ times the amplitude of the wave. There is a contribution from any slope of the surface over the 5-mm sampling length. R_a values of 0.4 μm mean that the sinusoidal waves have disappeared from the surface of the moulding, and only the inherent roughness from the mould surface and the gradual surface slope remain (see Table III).

Fig. 9 shows that there is a linear relation between the wavelength of the surface waves and their average roughness, for two packing pressures. Fig. 10 shows that the wavelength increases as the distance from the gate increases, which suggests either that the fountain flow differs in magnitude as the distance from the gate increases, or that the level of compressive stress in the surface layer decreases. Higher packing pressures produce lower R_a values on the surface. Fig. 10 shows that a packing pressure of 450 bar is not enough to remove the surface waves at the end of the moulding away from the gate, should the mould-filling velocity be low enough to allow the roughness to develop. Filling the mould at the highest velocity ($V = 7$) prevents the waves from appearing. Whether the disappearance of the waves is the result of inadequate time in the fountain flow for the waves to develop, or the waves being ironed out by the higher pressure gradients in rapid mould filling, is unknown.

The narrower MWD polystyrene has a greater wave amplitude at the same position on the moulding,

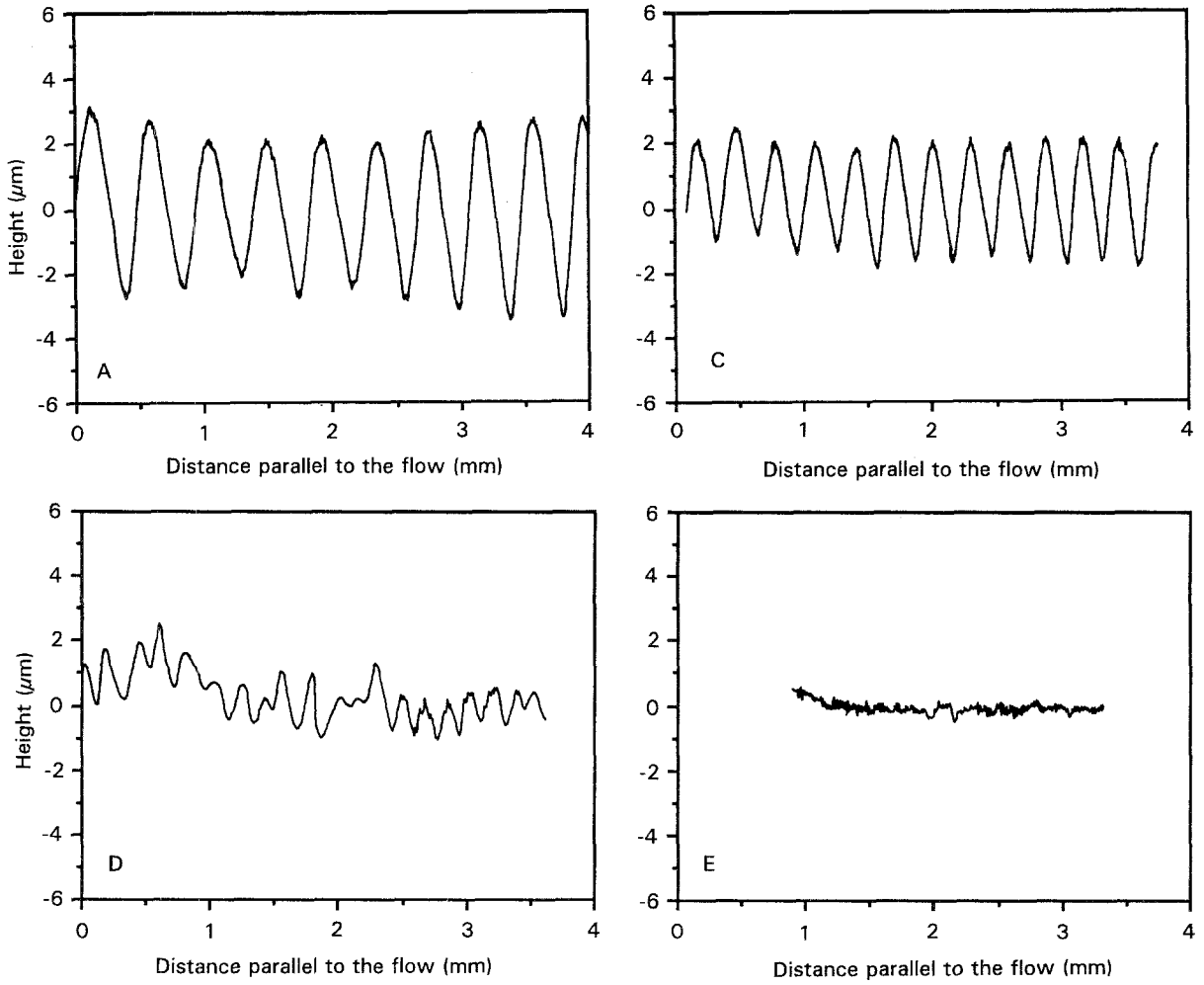

Figure 8 Talysurf traces for locations A, C, D, and E from the gate to the far end of the moulding (refer to Fig. 3 for locations) for the NMWD polystyrene, injection velocity 1, 60% packing pressure.

TABLE III Average roughness R_a (μm) as a function of moulding conditions and position on the bar

Specimen	Position on the bar				
	A	B	C	D	E
NB	2.55	1.99	1.39	0.44	0.44
NE	1.66	1.21	1.07	0.51	0.42
NG	0.37	0.40	0.34	0.44	0.43
WA	0.88	0.74	0.68	0.62	0.52
WE	0.83	0.98	0.93	0.54	0.63
WG	0.98	0.62	0.48	0.52	0.65
WJ	0.34	0.45	0.40	0.40	0.45

given the same moulding conditions. This shows that more than the melt elasticity is involved in the wave formation, because the two polymers have identical values of M_z/M_w and hence identical melt elasticity. The narrow-MWD polymer will have a higher viscosity at moderate shear rates than the wide-MWD polymer, and this could lead to higher tensile stresses in the shear flow of mould filling.

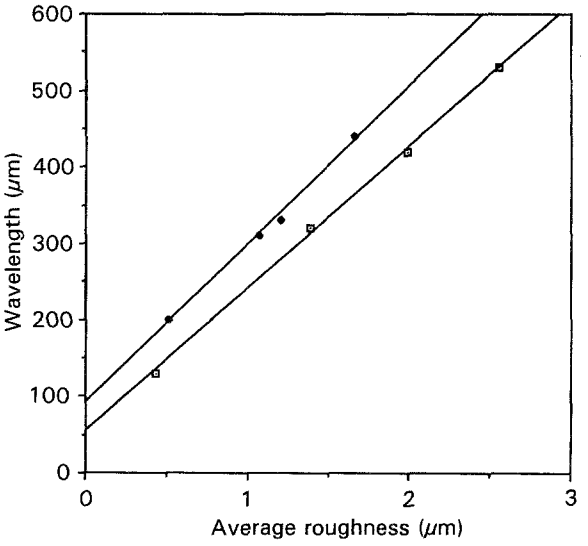

Figure 9 Relationship between wavelength and average roughness of the waves for NMWD polystyrene, injection velocity 1, and two packing pressures: ⊡, 5%; ◆, 60%.

4.2. Birefringence measurements of moulding skin

Measurements of the optical anisotropy of the mouldings has been used to determine both the orientation [3, 4] and the residual stresses [17] in glassy polymers. Ballman & Toor [3] found a low birefringence in the centre of the part, a maximum below the surface, and a low value at the surface. They proposed that this orientation distribution is the result of a solid layer along the mould wall, a linear shear-stress distribution in the flowing melt, and a fountain like motion at the front which deposits hot melt from the centre of the mould onto the wall, where it solidifies. Wales *et al.*

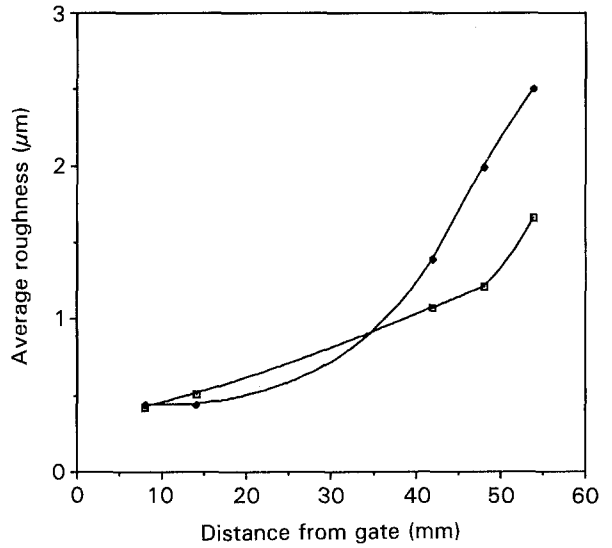

Figure 10 Average roughness R_a as a function of measurement position and packing pressure for the NMWD polystyrene at injection velocity 1, and two packing pressures: □, 40%; ◆, 5%.

[4] measured the flow birefringence of polystyrene during steady, isothermal shear flow and found that the value Δn_{FT} was related to the shear stress at the cavity wall, τ, by

$$\Delta n_{FT} = n_F - n_T = -1.0 \times 10^{-13} \tau^2 \quad (7)$$

The axis F is parallel to the flow, T is transverse to the flow and parallel to the mould surface, and N is normal to the mould surface. n_F is the refractive index for light polarized along the F axis. The units of shear stress in Equation 7 are $N\,m^{-2}$. When the equation is used with the estimated shear stress of $66\,kN\,m^{-2}$ when the mould is filled at a velocity of 1 unit, the predicted birefringence is 52×10^{-5}. Residual stresses will also contribute to the birefringence Δn_{FN}. The stress optical coefficient for polystyrene is relatively small at $9 \times 10^{-12}\,m^2\,N^{-1}$, so a surface residual stress of -5 MPa will contribute a birefringence of -4.5×10^{-5}.

The birefringence of solid samples can be measured in various ways. When the moulding is observed with plane-polarized light passing along the N axis the average of the values in the skins and core of the moulding is observed. Rectangular sections of thickness 1–2 mm were cut from the mouldings using a high-speed cutting wheel, then the surfaces were polished. The specimens were observed with monochromatic sodium light passing along the T axis, with the observation point being 12 mm from the end of the flow. The refractive indices do not vary along the T axis and the variation of Δn_{FN} with the distance from the surface of the bar is directly observed. Photographs were taken of the birefringence Δn_{FN} pattern through a Babinet compensator. The light passes through both the sample and a quartz wedge, and the photographs are crossed by equally spaced black fringes, which are contours of the total optical path difference for light polarized parallel and perpendicular to the orientation. Each black fringe is effectively a graph of the birefringence in the polystyrene as a function of the distance from the surface of the bar

TABLE IV Effect of the moulding conditions on the birefringence Δn_{FN} at the centre and surface of the section

V_{inj}	P_{inj} (%)	P_{hold} (%)	Central Δn_{FN} ($\times 10^{-5}$)	Surface Δn_{FN} ($\times 10^{-5}$)	Feature D depth (mm)
1	20	5	−23	−49	0.43
1	12	30	−14	−62	0.48
1	12	40	−16	−49	0.28? 0.77?
1	12	60	−12	−36	?
7	30	10	−13.2	−66	0.38
7	40	20	−19	−46	0.40
7	30	20	−8	−56	0.35

(?) Feature hard to identify.

(Fig. 11). For the high-filling-velocity samples there is a sharp increase in the slope of the birefringence graph at a distance D from the surface, whereas for the $V = 1$ samples the slope in this region is much less. The birefringence transition depth can be measured from the photographs taken through the Babinet compensator. Table IV shows that the depth is slightly thicker for the $V = 1$ samples than for the $V = 7$ samples. These distances can be compared with the solid-skin thicknesses calculated using Equation 3. As the measurement point is at 80% of the flow distance from the gate to the end of the flow, the flow will pass this point for 0.26 s when $V = 1$ (or possibly 1 s if the injection pressure is very low) and 0.037 s when $V = 7$. This means that the skin thickness is 0.18 and 0.07 mm for the two velocities, respectively.

Kamal & Tan [18] give precise identifications of various features in their birefringence thickness graphs for polystyrene moulded in a 1.8-mm-thick mould. The peak, A, of birefringence at the surface is related to the shear stress at the mould wall. A small minimum, B, always occurs about 0.04 mm from the surface, regardless of the distance from the gate, and they identify it with the thickness of the instantaneously frozen layer (from the fountain flow?). The maximum, C, somewhat deeper, is identified with the thickness of the skin at the moment of mould filling, and the slope change at D is tentatively identified with the solid-layer thickness at the moment of maximum packing pressure. Our measurement point is extremely close to the end of the mould and for the high filling velocity only the features A and D are observed, whereas for the $V = 1$ specimens the four features can be tentatively identified. The skin thickness from feature C in Fig. 6 is 0.14 mm, which is reasonably close to the predicted value.

The fringe order in the centre and at the skin of the specimens was found by using white light (which identifies the zero-order fringe as the only completely black fringe) and using the micrometer drive on the Babinet compensator to evaluate the partial fringe order. Table IV shows that the average birefringence values at the centre of the bar are slightly greater for the low injection velocity (-16 against -13×10^{-5}) while the surface values are slightly smaller (-48 against -56×10^{-5}). The surface birefringence of 52×10^{-5} at $V = 1$, predicted from the flow shear–stress using Equation 7, is very close to the

experimental values. There are no experimental pressure gradient values for $V = 7$, but it is expected that the shear-stress values would be higher and hence the flow birefringence considerably higher. Thus the agreement between theory and experiment may be fortuitous.

The effect of residual stresses on the birefringence variation is expected to be small as the stress optical coefficient of polystyrene is small. Sectioning experiments to remove the effect of residual stress were not carried out. There are contributions to the birefringence from the mould filling shear flow and from the compressive stresses in the melt in the surface layer. When the filling velocity is low, the shear stresses in the melt are low, the skin is thick and surface waviness occurs. Since the amplitude of the surface waves is less than 12 μm it is not likely that the buckling changes the surface stress distribution for a depth of more than 30 μm.

There is no sign of any special reduction in the birefringence at the surface for the $V = 1$ specimens. If the surface waves affect the birefringence distribution, it will only be for a depth that is 2 or 3 times the wave amplitude, e.g. for less than 0.03 mm. It is difficult at the low magnification used for the birefringence measurements to obtain data so close to the surface of the bar. Hence the birefringence distributions of these samples were similar to other observations [19] and do not throw any light on the mechanism of the surface wave formation.

4.3. Bending impact measurements

The equipment was based on an Avery Izod Impact Tester [14] with a modified pendulum constructed from laminated steel. A Kistler model 9321 quartz piezoelectric force cell was used to measure the force, and the nose of the striker was covered with a 1-mm layer of hard polyurethane rubber to reduce the impact oscillations. The output of the force cell was taken through a Kistler charge amplifier with a cut-off frequency of 180 kHz to a Datalab model 902 transient recorder with an eight-bit analogue to digital converter recording at 10-μs intervals. The data were analysed with a BBC micro computer and a maximum stress against maximum strain graph generated. The flexural strength was measured at various positions in the bar. The fracture plane in the unnotched specimens occurs at the level of the clamp, and this position was varied to be 10, 15, 20, 35 and 40 mm from the end of the moulded bar. The surface roughness was also measured at these positions.

Fig. 6 shows that significant non-linearity in the stress–strain curve occurred before the fracture. If the trace had been obtained from a tensile test the polymer would be judged to be on the point of yielding. Here there is evidence on the fracture surfaces that a craze has propagated a significant fraction of the cross section. As the stress analysis of the Izod test assumed linear elastic behaviour, the maximum stress values in Table V are only approximate. The real surface stress on the compressive side will be higher and that on the tensile side will be lower than the

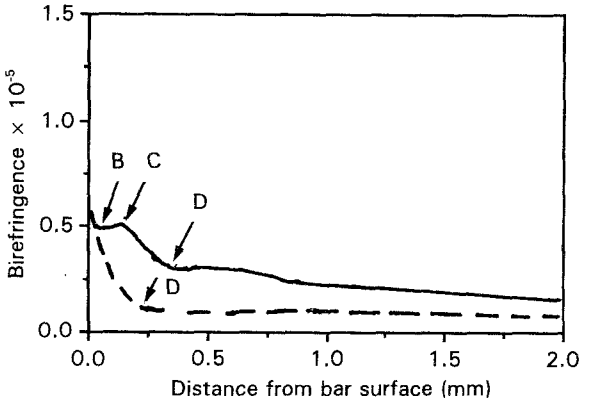

Figure 11 Birefringence Δn_{FN} variation through the thickness of the bar for (——) wavy surface, injection $V = 1$, packing pressure 40%; (– – – – –) smooth surface, $V = 7$, packing pressure 20%.

TABLE V Effect of surface roughness (R_a) on the Izod impact parameters

Injection velocity	Roughness R_a (μm)	Maximum stress (MPa)	Maximum strain (%)	Energy density (MJ m^{-3})
7	0.39	91.8	3.85	2.07
7	0.44	88.4	3.98	2.01
7	0.45	91.8	3.74	1.96
7	0.55	90.7	3.68	1.87
1	0.73	80.5	2.95	1.27
1	0.82	83.9	3.20	1.46
1	0.87	81.6	3.01	1.32
1	0.91	86.7	3.30	1.57
1	1.11	77.7	2.85	1.18
1	1.57	76.5	3.30	1.44

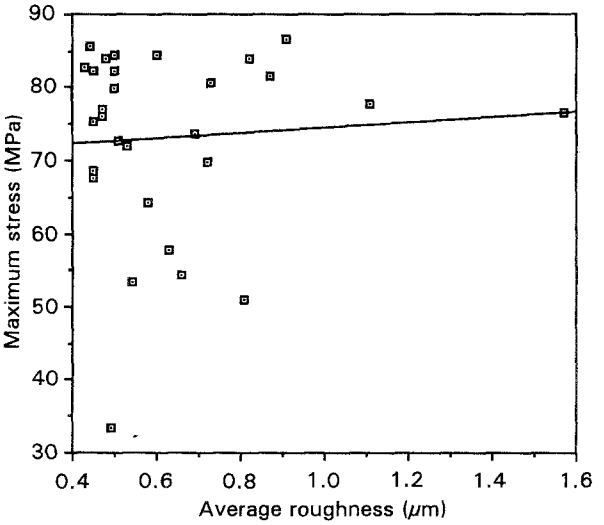

Figure 12 Variation of maximum stress in the Izod test with average roughness at the impact position.

tabulated values (see Fig. 5). The data can be used to evaluate the effect of surface roughness. Fig. 12 shows that the maximum stress has a slight positive correlation with the average roughness, but the correlation coefficient is only 0.07, which means that the relationship is due to chance.

The specimens moulded with low injection speeds have a discernible waviness on the surface. Equation 5 was used to calculate the stress concentration factor, q, of these waves. The result is that the biggest waves

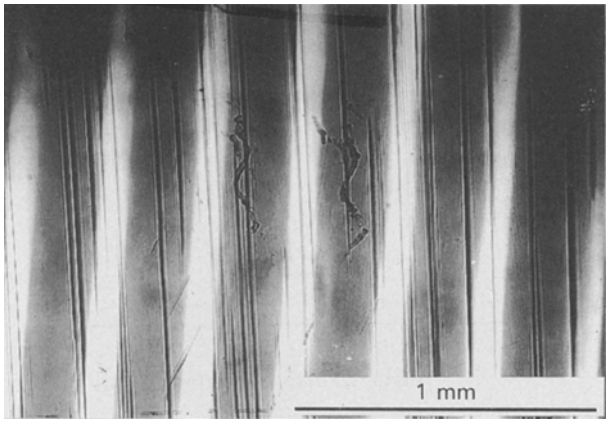

Figure 13 Reflected light micrograph of the crazed surface of a bar after the Izod test, showing that craze directions do not follow the wave fronts.

only produce a stress concentration factor of 1.14. Crazes are visible in fractured specimens and the crazing extends up the bars from the clamping position. When the tensile surfaces of fractured specimens were examined under an optical microscope the appearance was as in Fig. 13. If the surface roughness causes a significant stress concentration, the crazes should form only in the wave valleys (the bright regions). However the crazes formed both in the valleys and the peaks, and the craze planes are not parallel to the wave front, tending to be perpendicular to the principal tensile stress.

The lack of correlation between the surface roughness and the maximum stress in the Izod test is due to a number of factors. The average birefringence of the bars has a bigger effect on the maximum stress, and no doubt there are changes in the residual stresses as a result of the changes in processing conditions. The lack of coincidence between the craze-surface direction and the wave fronts suggest strongly that the surface waves play no part in the growth of crazes to the millimetre size that they have when the bar fractures. In all our tests, the melt flow orientation was parallel to the tensile stress in the bent bar. If tests were carried out with the stress applied in the weak direction, which would mean that the stress would be parallel to the wave fronts, the correlation between the impact strength and the surface roughness would be even less than found here.

5. Discussion

Large changes in molecular orientation and surface quality occur as a result of the variations in the injection-moulding conditions. The present study shows that the surface quality is improved by having a high injection speed, and that a high packing pressure can produce minor improvements in the surface quality. The proposed mechanism for the formation of the surface waves is buckling caused by the compressive melt stresses in the fountain flow region. The amplitude of the waves increases with the time for which the melt is in the fountain-flow region. This time is relatively small, given that the entire mould fills in between 1.3 and 5 s when the injection speed is at its lowest setting. In short-shot mouldings, the length of the region that does not touch the mould wall is about 3 mm. It is possible that the shape of the flow front changes when the injection stroke is stopped, because the melt is relatively compressible. Nevertheless if the flow front is 2 mm long in a mould of length 60 mm from the gate, the polymer is in the fountain-flow region for the order of 0.1 s. For the polystyrene studied, it would appear that the waves do not form if the melt is in the fountain-flow region for less than 0.01 s. It would be of interest to repeat the experiments with polymers of higher or lower viscosity to see the effect of the melt viscosity in preventing the waves forming; however changes in viscosity are nearly always associated with changes in melt elasticity, so careful experimental design would be necessary. The tensile and compressive stresses in a shear flow are a result of melt elasticity. The melt compliance of polystyrene is high because the entanglement molecular weight in the melt is relatively high. Nevertheless surface waves are observed on injection mouldings from polycarbonate, which has a much lower melt compliance than polystyrene.

The bending impact strength of unnotched polystyrene is likely to be controlled by molecular orientation, and the evidence here is that it is not controlled by surface roughness. The surface roughness is a by-product of the processing conditions. The usual advice for injection moulding polystyrene is to use a high injection speed; this will minimize the thickness of the oriented skin on the mouldings as well as increasing the productivity of the mould. One useful effect of the high injection speed will be to minimize the surface roughness.

References

1. R. S. SPENDER and G. D. GILMORE, *Modern Plastics* **28** (1950) 97.
2. G. B. JACKSON and R. L. BALLMAN, *SPE. J.* **16** (1960) 1147.
3. R. L. BALLMAN and H. L. TOOR, *Modern Plastics* **38** (1960) 113.
4. J. L. S. WALES, J. VAN LEEIWAN and R. VAN DER VIGH, *Polym. Eng. Sci.* **12** (1972) 358.
5. N. J. MILLS, *Plast. Rubber Proc. Appl.* **3** (1983) 181.
6. K. N. HUNT, J. R. G. EVANS and N. J. MILLS, *J. Mater. Sci.* **26** (1991) 5229.
7. H. HOGBERG, *Modern Plastics* **33** (1955) 150.
8. C. D. HAN and C. A. VILLAMIZAR, *Polym. Eng. Sci.* **18** (1978) 173.
9. W. DIETZ, J. L. WHITE and E. S. CLARK, *ibid.* **18** (1978) 273.
10. J. L. WHITE and W. DIETZ, *ibid.* **19** (1979) 1081.
11. J. L. WHITE, *ibid.* **15** (1975) 44.
12. D. HANDS, *Rubber Chem. Technol.* **50** (1977) 480.
13. N. J. MILLS, *J. Mater. Sci.* **17** (1982) 558.
14. N. J. MILLS and P. S. ZHANG, *ibid.* **24** (1989) 2099.
15. R. P. KAMBOUR, *J. Polym. Sci. Macromolec. Rev.* **7** (1973) 1.
16. N. J. MILLS, *Eur. Polym. J.* **5** (1969) 675.
17. L. J. BROUTMAN and S. M. KRISHNAKUMAR, *Polym. Eng. Sci.* **16** (1976) 74.
18. M. S. KAMAL and V. TAN, *ibid.* **19** (1979) 58.

Received 30 March
and accepted 19 October 1993